Molecular Dynamics Simulation of Structure, Thermodynamic, and Dynamic Properties of Poly(dimethylsilamethylene), Poly(dimethylsilatrimethylene) and Their Alternating Copolymer

Zoi A. Makrodimitri, Vasilios E. Raptis,† and Ioannis G. Economou*

Molecular Thermodynamics and Modeling of Materials Laboratory, Institute of Physical Chemistry, National Center for Scientific Research "Demokritos", GR-153 10 Aghia Paraskevi Attikis, Greece

Received: March 24, 2006; In Final Form: May 26, 2006

Molecular dynamics is used for the simulation of silicon-containing polymers with promising membrane material properties. An atomistic force field is developed for the description of bond bending, torsional angle variation, and nonbonded intra- and intermolecular interactions. Detailed ab initio quantum mechanics calculations on corresponding monomers that appeared recently in the literature are used for the parametrization of the bonded and nonbonded local intramolecular force field. For the intermolecular and nonbonded nonlocal intramolecular interactions, parameters are obtained from accurate force fields proposed in the literature for similar compounds. The force field is used subsequently for the calculation of thermodynamic, structure, and dynamic properties of two homopolymers, namely, poly(dimethylsilamethylene) and poly(dimethylsilatrimethylene), and their alternating copolymer. A wide range of temperatures and pressures is examined. Polymer systems of different molecular weights are simulated. Experimental data available for these polymers are very limited. In all cases, simulation results are in good agreement with these data. Furthermore, simulation results agree very well with empirical macroscopic correlations used widely for rubbery polymers for the properties under consideration.

1. Introduction

The tremendous increase of computing power at relatively low price and advances in applied statistical mechanics in recent years have made molecular simulation a powerful tool for the elucidation of microscopic phenomena that control macroscopic properties and the subsequent prediction of such properties for a wide range of complex materials, including fluid mixtures, polymers, solids, and so forth.[1,2] In this way, molecular simulation contributes greatly to the development of quantitative microscopic structure−macroscopic property relationships and to the design of novel materials with tailor-made end-use properties for a wide range of applications.

Macromolecular systems are of major interest from the scientific and technological point of view. Their macroscopic thermodynamic, transport, mechanical, optical, electrical, and other properties depend on the underlying long chain architecture, micro- and mesostructures. Considerable effort has been devoted toward the development of molecular simulation methods, mostly Metropolis Monte Carlo (MC) simulation and molecular dynamics (MD), suitable for the study of polymers in melt, in solution, in blend, and so forth.[3,4] MC simulation is a stochastic method that allows efficient sampling of phase space. On the basis of "elementary" moves, the system visits many important configurations that have significant contribution to the macroscopic properties of interest.[5] A number of powerful "elementary" moves were proposed in recent years that allow efficient sampling of important polymer configurations and, thus, result in reliable predictions within reasonable simulation time.[6−13]

A major limitation of the MC methods is that they cannot be used for time-dependent properties, such as transport and dynamic properties. MD provides the means for monitoring the evolution of the system with time and calculation of relevant properties.[1] Furthermore, with the use of state-of-the art computing facilities, one may simulate several microseconds of real time.[14] Simulation over such time scales allows for the reliable calculation of a wide range of macroscopic properties, at least for low and medium molecular weight values of rubbery polymers.

MD has been used extensively for the simulation of polyolefins of variable chemical and macromolecular architecture,[15−18] other nonpolar polymers[18,19] as well as polar polymers.[20] A relatively unexplored class of rubbery polymers consists of poly(silamethylenes), most of them with low glass transition temperature values. These polymers have shown promising membrane properties for light gas and hydrocarbon separation.[21,22] A systematic experimental investigation of poly(dimethylsilamethylene) (PDMSM), poly(dimethylsilatrimethylene) (PDMSTM), and their copolymers of different compositions in mixtures with *n*-alkanes revealed permeability property values, that is, solubility coefficient and diffusion coefficient, which make them suitable to use as membrane materials.[23] Such macroscopic physical properties are governed by the microscopic structure of the polymers. Consequently, thorough elucidation of such a structure provides the basis for accurate prediction of macroscopic properties. MD using a realistic united-atom (UA) force field for PDMSM and hydrocarbon molecules was in good agreement with experimental data for the PDMSM melt and

* To whom correspondence should be addressed. E-mail: economou@chem.demokritos.gr.

† Current address: Department of Chemistry, University of Ioannina, GR-45 110 Ioannina, Greece.

10.1021/jp061841g CCC: $33.50
Published on Web 07/21/2006

the PDMSM−hydrocarbon mixtures.[24,25] PDMSM has been simulated also at a more coarse grained level, and results were found in reasonably good agreement with experiment.[26]

This work focuses on the two homopolymers, PDMSM and PDMSTM, as well as their 50:50 alternating copolymer (see Figure 1). The UA force field for the bonded and local intramolecular interactions is based on recent detailed ab initio calculations and is slightly different from an earlier force field for PDMSM based on preliminary ab initio calculations.[24] For the nonlocal intramolecular interactions and the intermolecular interactions, the Lennard-Jones parameters proposed for the methylene (CH_2) UA in *n*-alkanes[27] and for Si in poly(dimethylsiloxane)[28] are used, while methyl (CH_3) parameters are adjusted to match the experimental density for PDMSM. MD simulations are performed over a wide range of temperature and pressure conditions and of polymer molecular weight values. Microscopic structure, conformational properties, and macroscopic thermodynamic and dynamic properties are calculated. It is expected that this systematic characterization of the polymer melts can provide valuable insights toward the subsequent prediction of mixture properties and ultimately the use of such polymers as membrane materials.

2. Force-field Development

Intra- and intermolecular interactions exhibited by the polymer molecules are described based on a UA force field. In the UA representation, light atoms (in this case hydrogens) are not accounted explicitly. Consequently, the polymer chains in this work consist of CH_3 groups, CH_2 groups, and Si atoms. When appropriate parametrization of the model is used, accurate results are obtained with a substantial decrease of computing time compared with an all-atom representation. In the force field developed, the potential energy function is written as the sum of contributions due to bond stretching, bond-angle bending, dihedral angle torsion, and nonbonded intra- and intermolecular interactions, according to the expression

$$V_{\text{total}}(\mathbf{r}_1,...,\mathbf{r}_N) = V_{\text{stretching}} + V_{\text{bending}} + V_{\text{torsion}} + V_{\text{nonbonded}}$$
$$= \sum_{\text{all bonds}} V(l_i) + \sum_{\text{all bond angles}} V(\theta_i) + \sum_{\text{all torsional angles}} V(\phi_i) + \sum_{\text{all pairs}} V(r_{ij})$$
$$= \sum_{\text{all bonds}} \frac{k_{l_i}}{2}(l_i - l_{i,o})^2 + \sum_{\text{all bond angles}} \frac{k_{\theta_i}}{2}(\theta_i - \theta_{i,o})^2$$
$$+ \sum_{\text{all torsional angles}} \frac{1}{2}k_\phi(1 - \cos 3\phi) + \sum_{\text{all pairs}} 4\epsilon_{ij}\left[\left(\frac{\sigma_{ij}}{r_{ij}}\right)^{12} - \left(\frac{\sigma_{ij}}{r_{ij}}\right)^{6}\right] \quad (1)$$

where l_i, θ_i, and ϕ_i denote bond length, bond angle, and torsional angle, respectively, and r_{ij} is the distance between interaction sites *i* and *j*. Flexible bonds are used, and the potential energy of each bond is evaluated by using a simple harmonic potential. Similarly, bond-angle fluctuations around the equilibrium angle θ_o are subject to harmonic fluctuations. For all dihedral angles, a 3-fold symmetric torsional potential is used with $\phi = 0^o$ denoting a trans state. Finally, nonbonded interactions are described by a Lennard-Jones potential, $V_{LJ}(r)$. $V_{LJ}(r)$ describes all intermolecular site−site interactions as well as intramolecular interactions between sites separated by three or more bonds.

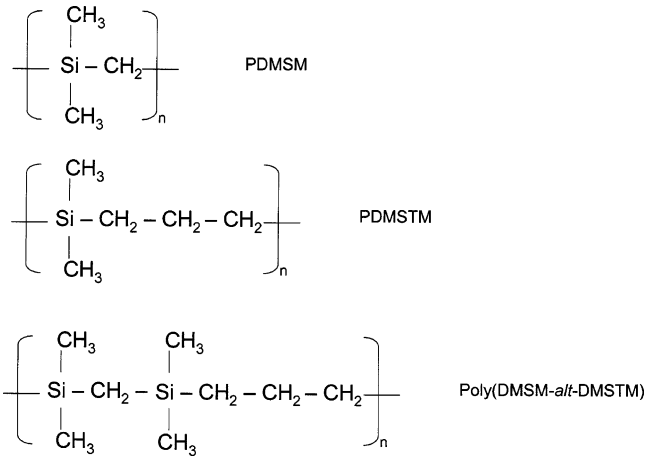

Figure 1. Chemical structures of the polymers examined in this work.

Standard Lorentz−Berthelot combining rules are used to describe nonbonded interactions between sites of different types

$$\epsilon_{ij} = \sqrt{\epsilon_{ii}\epsilon_{jj}} \quad (2a)$$

and

$$\sigma_{ij} = (\sigma_{ii} + \sigma_{jj})/2 \quad (2b)$$

Two parameter sets are employed in this model, namely, *local* and *nonlocal* ones. The local parameters refer to bonded interactions, that is, stretching, bending, and torsion interactions. They also include intramolecular nonbonded interactions between sites separated by three or four consecutive bonds. The nonlocal parameters describe the remaining of the nonbonded interactions, that is, intramolecular interactions between sites that are separated by more than four bonds and intermolecular interactions.

The two parameter sets were evaluated using two different types of calculations. More specifically, ab initio quantum mechanical calculations were performed to determine the local parameters, whereas MD calculations were fit to literature data for PDMSM volumetric properties to evaluate the nonlocal parameters for CH_3.

Ab initio calculations were performed to describe the conformational energy surface of di(trimethylsilyl)methane (DTMSM) and trimethylpropylsilane (TMPS), which are the PDMSM dimer and PDMSTM monomer, respectively. All different types of local interactions in the polymer, that is, stretching, bending, torsions, and nonbonded interactions, exist in these two molecules that have a moderate size so that they can be subjected to high-level quantum mechanical calculations with reasonable CPU time and memory requirements. Details on these calculations can be found elsewhere,[29] and only a brief description is presented here.

Second-order Møller−Plesset, MP2, theory[30] was employed in all ab initio calculations using 6-311G,[31] a triple split valence basis set assuming three sizes of contracted functions for each atomic orbital type. The selected basis set does not include diffuse or polarizations functions, since the systems are neutral and contain no lone pair electrons. To ensure suitability of this basis set, a number of calculations were repeated for DTMSM, using 6-311G*, and yielded identical results in terms of energy and geometry. All the electrons were included in the correlation calculations, and zero-point energy was calculated.

The DTMSM minimum energy configuration was sought by means of MP2/6-311G calculations, with respect to all degrees of freedom. Then, constrained energy minimization calculations

at the same level of theory followed for a complete determination of the energy differences between the global minimum geometry and other representative configurations. In those calculations, two $CH_3-Si-CH_2-Si$ dihedral angles arbitrarily denoted as "main" were fixed at various values. Starting from the all-trans configuration, each main dihedral angle was varied in a stepwise manner by 30°. Thanks to the high symmetry of the DTMSM molecule in its UA representation, 10 such conformations are sufficient for a representative picture of the conformational subspace defined by the main dihedral angles.

To obtain a more detailed picture of the configuration space, a set of additional constrained calculations were performed, with the main torsion angles fixed at their trans conformation, and selected bond angles constrained at values differing by ±1, ±2, and ±3° from their value at the all-trans configuration. The all-trans configuration was selected as a reference state for bond-angle calculations to decouple the torsion from the rest of the potential energy components, since bonds connecting two sp^3 hybridized atoms, like Si and C, are expected to contribute to zero torsion energy when they are in a trans state.[32] To cover all types of bond angles present in DTMSM, the Si−C(central)−Si angle, C(methyl)−Si−C(methyl) angle, and the C(methyl)−Si−C(central) angle were studied in the above calculations.

A remarkable feature of the results was that the global minimum energy DTMSM structure is characterized by a value of about ±16° for both main torsion angles, whereas the all-trans state represents a rather flat saddle point. Such structural characteristics have been reported for other short-branched polymers such as poly(isobutylene),[33] poly(vinylidene chloride),[33] and poly(dimethylsilane)[34] and it is due to the repulsion among methyl groups attached to each of the Si atoms.

Force-field local parameters were fit to MP2 calculations by minimizing the following objective function

$$F = \frac{\sum_{i=1}^{N_{conf}} (V_i^{MP2} - V_i^{FF}(\mathbf{p};\mathbf{r}_i))^2}{\sum_{i=1}^{N_{conf}} (V_i^{MP2})^2} \quad (3)$$

where V_i^{MP2} represents the quantum mechanical energy with respect to the minimum structure and V_i^{FF} represents the force-field energy of the ith configuration based on single molecule molecular mechanics calculations. The force-field parameters are collectively denoted by $\mathbf{p}$ and are allowed to vary during the minimization procedure, whereas $\mathbf{r}_i$ refers to the quantum mechanically determined atomic coordinates of the ith configuration, which are held fixed throughout the calculation.

The $Si-C(CH_2$ or $CH_3)$ bond stretching constant k_{l_i}, equilibrium bond length $l_{i,o}$ and intrinsic torsion energy barrier k_{φ}, the $Si-CH_2-Si$, $CH_2-Si-CH_3$ and $CH_3-Si-CH_3$ angle bending constants k_{θ_i} and equilibrium values $\theta_{i,o}$, as well as the Si and CH_3 sites Lennard-Jones local parameters ϵ and σ were determined at this stage.

The same procedure was used subsequently for TMSP. Again, a global minimization MP2/6-311G computation was performed, and then, constrained minimizations at the same level of theory followed where the main dihedral angles were fixed. The $CH_3-CH_2-CH_2-Si$ and one of the $CH_2-CH_2-Si-CH_3$ angles were chosen as the "main" dihedral angles and were varied by 30° in each minimization calculation starting from the all-trans conformation. This molecule is characterized by a lower symmetry than that of DTMSM, therefore an augmented set of 26 fixed dihedral configurations was employed to adequately span the conformation space. No fixed bond-angle calculations were performed this time. The rest of the calculations details were the same as those in the DTMSM case. The all-trans conformation was found to be the TMSP potential energy global minimum.

The DTMSM force-field parameters were assumed to be transferable to TMSP, so that a much smaller number of additional parameters were determined. More specifically, the following force-field parameters were evaluated: $C(CH_3$ or $CH_2)-C(CH_3$ or $CH_2)$ bond stretching constant k_{l_i}, equilibrium bond length $l_{i,o}$ and intrinsic torsion energy barrier k_{φ}, $CH_3-CH_2-CH_2$ and CH_2-CH_2-Si angle bending constants k_{θ_i} and equilibrium values $\theta_{i,o}$, and CH_2 local Lennard-Jones parameters ϵ and σ.

To evaluate the accuracy of the newly developed force field for thermodynamic property predictions, 6 ns long MD runs were performed at the isothermal−isobaric (*NPT*) ensemble at conditions where densities are known experimentally, that is, at 293.15 K and 0.1 MPa for liquid DTMSM[35] and at 273.15 K and 0.1 MPa for liquid TMSP.[36] Nonlocal parameters developed previously for PDMSM[24] were employed at this stage for intermolecular interactions. Density was predicted within an error of less than 1%.

The Lennard-Jones parameters for the nonlocal interactions of PDMSM were estimated as follows: For Si, the ϵ and σ parameters proposed by Sok et al.[28] for poly(dimethylsiloxane) were adopted. For CH_2, the TraPPE ϵ and σ parameters were used.[27] TraPPE is a very accurate UA force field for *n*-alkanes, alkenes, and other organic compounds. In TraPPE, σ for CH_3 is smaller than σ for CH_2, which is physically unrealistic. Consequently, CH_3 parameters were adjusted here so that the force field reproduces accurately the experimental density of PDMSM at ambient conditions and, at the same time, $\sigma_{CH_3} > \sigma_{CH_2}$.

For PDMSTM, there are no experimental thermodynamic data available. Consequently, by assuming that the nonlocal Lennard-Jones parameters for PDMSM are transferable to other polymers of similar chemical structure, these parameters were used also for PDMSTM. Finally, for the alternating copolymer, the force-field parameters for the corresponding homopolymers were used. To summarize, the parameters for the force field developed in this work are shown in Table 1.

3. Simulation Details

In this work, all MD simulations were performed at the isobaric−isothermal (*NPT*) ensemble using Nosé and Klein extended method.[37−39] In this case, the Lagrangian assumes the form

$$\mathcal{L} = \sum_i \frac{m_i}{2} s^2 \dot{r}_i^2 - V_{total} + \frac{Q}{2}\dot{s}^2 - g k_B T \ln s + \frac{9}{2} W L^4 \dot{L}^2 - P_{ext} L^3 \quad (4)$$

where $g = 3nN_{ch} + 1$ is the number of degrees of freedom of the system, n is the number of atoms of each chain, N_{ch} is the number of chains, L is the box edge length, s is the "bath" degree of freedom used to control the temperature, W and Q are the inertia parameters associated with L and s, respectively, and P_{ext} is the externally set pressure. Equations of motions are derived from the Lagrangian of the extended ensemble. A fifth-order Gear predictor−corrector scheme[40] was used to integrate the equations of motion in Cartesian coordinates. The values

TABLE 1: Atomistic UA Force Field for PDMSM, PDMSTM, and Poly(DMSM-*alt*-DMSTM)

Type of interaction	*Potential function and parameters*			
Bond stretching	$V_{stretching}(l) = 1/2k_l(l - l_o)^2$			
	Bond	k_l (kcal/mol/Å^2)	l_o (Å)	
	C-C	192.0	1.539	
	Si-C	123.2	1.917	
Bond bending	$V_{bending}(\theta) = 1/2k_\theta(\theta - \theta_o)^2$			
	Bond angle	k_θ (kcal/mol deg^2)	θ_o (deg)	
	CH_2-Si-CH_2	0.0315	111.6	
	CH_2-Si-CH_3	0.0315	111.6	
	CH_3-Si-CH_3	0.0282	98.2	
	Si-CH_2-Si	0.0372	119.2	
	Si-CH_2-CH_2	0.0272	107.7	
	CH_2-CH_2-CH_3	0.0378	115.0	
	CH_2-CH_2-CH_2	0.0378	115.0	
Dihedral angles	$V_{dihedral} = 1/2k_\varphi(1-cos3\varphi)$			
	Dihedral angle	k_φ (kcal/mol)		
	C-C	2.331		
	Si-C	0.735		
Non bonded interactions	$V_{LJ}(r_{ij}) = 4\varepsilon[(\sigma_{ij}/r_{ij})^{12} - (\sigma_{ij}/r_{ij})^6]$			
		Local parameters		Non- local parameters
	UA	σ (Å)	ε (kcal/mol)	σ (Å)	ε (kcal/mol)
	Si	2.369	0.791	3.385	0.585
	CH_2	3.407	0.289	3.950	0.091
	CH_3	3.407	0.289	4.150	0.210

of the parameters *W* and *Q* were the same as those of previous work on PDMSM and on polypropylene.[24,41]

In all of the systems simulated, the number of chains was chosen so that the total number of UAs in the simulation box was on the order of 800−1000. The initial configurations were obtained using the Cerius^2 software package of Accelrys Inc. and were subjected to molecular mechanics.[42] An "equilibration" MD stage of 1 ns was performed followed by a production run of 5 ns for the calculation of thermodynamic properties. The integration time step was always equal to 0.5 fs to ensure system stability over time (percentage deviation between predicted and corrected accelerations less than 5×10^{-3}). For the calculation of dynamic properties, much longer simulations, often exceeding 100 ns, were performed. In all cases, periodic boundary conditions were applied to the simulation box, whose size was allowed to fluctuate during the run. In all cases, the box length was ca. 31 Å. A Verlet neighbor list[1] and a truncated Lennard-Jones potential were used to speed up calculation of interactions between molecules. In the present work, the potential tail beyond $r = 1.45\sigma$ was substituted by a fifth-order polynomial, whose value beyond $r = 2.33\sigma$ is equal to zero. The instantaneous pressure of the system P_{int} was calculated during the simulation according to the molecular virial expression proposed by Theodorou et al.[43] The "tail" contributions to the internal energy and to the pressure were taken into account.[44]

4. Results and Discussion

A. Thermodynamic Properties. The *PVT* properties of PDMSM, PDMSTM, and poly(DMSM-*alt*-DMSTM) in melt were simulated over an extensive temperature and pressure range, that is, from 300 to 400 K and from 0.1 to 160 MPa. For PDMSM, the system simulated consisted of 3 chains with 80 monomeric units, so the molecular weight was 5776. For PDMSTM, the system consisted of 3 chains with 40 monomeric units and the molecular weight was 4016. Finally, for the copolymer, simulation was performed on a system with 3 chains of 27 monomeric units each that corresponds to a molecular weight of 4660.

In Table 2, MD simulation results are presented. For any given temperature and pressure, $\rho_{PDMSM} > \rho_{copolymer} > \rho_{PDMSTM}$. In other words, the increase in the number of methyl groups attached to the backbone results in an increase in density. At the same time, the fraction of Si atoms, that are heavier than CH_2 and CH_3, is higher in the PDMSM chain compared to the PDMSTM chain, while σ for Si is lower than σ for CH_2 and CH_3. Both facts contribute to a higher density for the former polymer. In Figure 2, the melt density of the three polymers at 0.1 MPa is shown as a function of temperature. Experimental data for PDMSM and copolymer are also shown.[22,23,45−47] The agreement between experimental data and simulation is very good in all cases. For PDMSM in particular, the melt density

TABLE 2: Density of PDMSM, PDMSTM, and Poly(DMSM-*alt*-DMSTM) (copoly) from MD Simulation at Various Temperatures and Pressures[a]

	density (g/cm^3)								
	300 K			350 K			400 K		
P (MPa)	PDMSM	PDMSTM	copoly	PDMSM	PDMSTM	copoly	PDMSM	PDMSTM	copoly
0.1	0.918_1	0.885_1	0.898_2	0.893_2	0.858_1	0.875_2	0.871_1	0.832_1	0.851_1
80	0.943_2	0.915_1	0.929_3	0.925_1	0.893_1	0.909_1	0.905_2	0.873_1	0.888_1
160	0.961_2	0.936_3	0.955_1	0.951_1	0.919_1	0.933_1	0.931_2	0.901_1	0.915_1

[a] The subscript indicates the statistical uncertainty in the last decimal point.

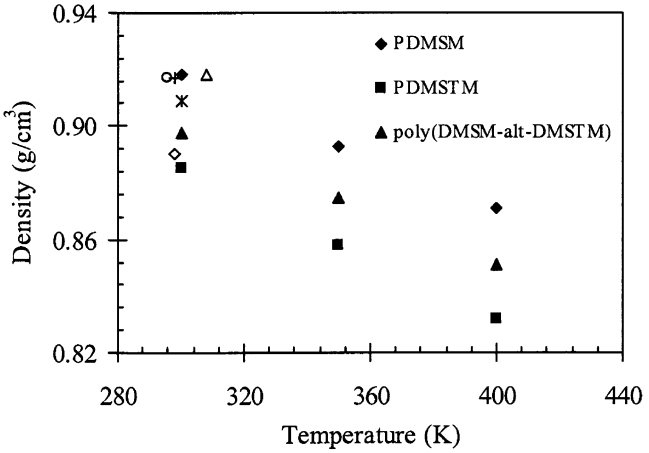

Figure 2. Melt densities of PDMSM, PDMSTM, and poly(DMSM-*alt*-DMSTM) at 0.1 MPa and different temperatures: experimental data for PDMSM (circles from ref 22, cross from ref 47, stars from ref 45, and upper triangles from ref 46), for the copolymer (diamonds from ref 23), and MD predictions (filled points).

at 300 K has been measured by several authors. The force field developed here predicts a density value which agrees within experimental uncertainty with some of these data. This is a clear improvement over an earlier model whose predictions agreed within 2% with experimental data.[24] Experimental densities are not available at elevated pressures for any of these polymers.

The volume fluctuations recorded in the course of *NPT* MD simulations were used to calculate the isothermal compressibility, κ_T, for the three polymer melts, according to the expression

$$\kappa_T = -\frac{1}{V}\left(\frac{\partial V}{\partial P}\right)_T = \beta\frac{\langle V^2\rangle - \langle V\rangle^2}{\langle V\rangle} \tag{5}$$

Simulation results are shown in Table 3. No experimental data are available for these polymers. However, the κ_T simulation values are in the range $(2-6) \times 10^{-4}$ MPa^{-1}, which is a typical range for many known polymers.[48]

Furthermore, the solubility parameter was calculated from the expression

$$\delta = \sqrt{\left\langle\frac{E_{\mathrm{coh}}}{V}\right\rangle} \tag{6}$$

E_{coh} is the cohesion energy of the system and is estimated as the difference between the intramolecular energy of all "parent" chains and the total potential energy of the simulation box, by taking potential "tail" contributions into account.[49] Simulation results are shown in Table 4.

The effect of molecular weight on the thermodynamic properties of the three polymers was examined in detail. MD simulations for systems of different chain lengths were performed. In Table 5, the characteristics of the different systems examined are shown.

The melt density for the three polymers at 0.1 MPa and at 300 and 400 K is shown in parts a and b of Figure 3 respectively. In all cases, density increases with molecular weight, for the molecular weight range examined. At high enough molecular weight, the density reaches a limiting value. This behavior can be expressed with the following simple empirical expression[48]

$$\rho = \rho_\infty - \frac{A}{MW} \tag{7}$$

where ρ_∞ is the value of density at infinite chain length and A is a constant. Simulation results in Figure 3 are correlated very well with eq 7. The infinite chain length densities obtained from this correlation are the following: for PDMSM, $\rho_\infty = 0.924$ g/cm^3 (at 300 K), 0.875 g/cm^3 (at 400 K); for PDMSTM, $\rho_\infty = 0.891$ g/cm^3 (at 300 K), $\rho_\infty = 0.839$ g/cm^3 (at 400 K); and for poly(DMSM-*alt*-DMSTM), $\rho_\infty = 0.857$ g/cm^3 (at 400 K).

Similarly, the molecular weight dependence of the solubility parameter was estimated as shown in Figure 4 for the two homopolymers. For PDMSM, the extrapolated value at infinite molecular weight is equal to 8.08 (cal/cm^3)$^{1/2}$ and agrees remarkably well with the experimental value of 8.02 (cal/cm^3)$^{1/2}$.[47] For PDMSTM, the infinite molecular weight value is equal to 7.55 (cal/cm^3)$^{1/2}$. Experimental δ values for PDMSTM are not available in the literature. On the basis of these simulations, it is concluded that PDMSM is more cohesive compared with PDMSTM.

B. Structure Properties. The structure of polymer melts was examined by calculating the intramolecular pair density function $w(r)$ and the intermolecular pair distribution function $g(r)$. In Figure 5, the total intermolecular pair distribution function for the three polymers of the highest molecular weight examined at 300 K and 0.1 MPa is shown. In all cases, a strong "correlation hole effect" is pronounced. At small distances, $g(r)$ is well below 1, because the cloud of segments belonging to the reference chain excludes segments of other chains from approaching the reference segment. This behavior has also been observed for polyolefins.[50,51] Examination of this figure indicates that the chains of PDMSTM have more intermolecular contacts compared to the chains of the other two polymers at the same distance. This microscopic behavior is consistent with the macromolecular architecture of PDMSTM that has fewer substituents in the chain leading to more intermolecular neighbors.

The distance over which the "correlation hole effect" exists scales with the size of the chain, as shown in Figure 6 where the total intermolecular pair distribution function for various molecular weights of PDMSTM at 300 K and 0.1 MPa is shown. Furthermore, an increase in the chain length results in a small shift of the first peak position to lower distances, due to an increase of the density, which results to closer packing.

TABLE 3: Isothermal Compressibility, κ_T, of PDMSM, PDMSTM, and Poly(DMSM-*alt*-DMSTM) (copoly) from MD Simulation at Various Temperatures and Pressures

	isothermal compressibility ($\times 10^4$ MPa^{-1})								
	300 K			350 K			400 K		
P (MPa)	PDMSM	PDMSTM	copoly	PDMSM	PDMSTM	copoly	PDMSM	PDMSTM	copoly
0.1	3.6	4.8	5.8	4.7	6.6	5.9	6.1	6.1	5.9
80	2.2	3.0	3.1	2.9	4.7	4.0	4.1	5.2	5.2
160	2.1	2.9	1.9	2.6	3.0	2.8	3.1	2.9	3.0

[a] Statistical uncertainty in all cases is $(0.5-1) \times 10^{-4}$ MPa^{-1}.

TABLE 4: Solubility Parameter, δ, of PDMSM, PDMSTM, and Poly(DMSM-*alt*-DMSTM) (copoly) from MD Simulation at Various Temperatures and Pressures[a]

	solubility parameter (cal/cm^3)$^{1/2}$								
	300 K			350 K			400 K		
P (MPa)	PDMSM	PDMSTM	copoly	PDMSM	PDMSTM	copoly	PDMSM	PDMSTM	copoly
0.1	7.85_7	7.59_2	7.63_6	7.55_3	7.42_3	7.39_5	7.32_3	7.06_4	7.09_5
80	8.09_2	8.14_3	7.84_2	7.89_4	7.74_4	7.83_5	7.65_3	7.64_5	7.42_2
160	8.24_3	8.25_3	8.26_2	8.18_2	8.04_2	7.84_2	7.91_5	7.95_2	7.78_5

[a] The subscript indicates the statistical uncertainty in the last decimal point.

TABLE 5: Characteristics of the Simulated Homopolymer and Copolymer Melt Samples

chain size	number of chains	molecular weight
	PDMSM	
5mers	48	376
10mers	24	736
20mers	12	1456
40mers	6	2896
80mers	3	5776
	PDMSTM	
5mers	31	516
10mers	16	1016
20mers	8	2016
40mers	3	4016
	poly(DMSM-*alt*-DMSTM)	
3mers	30	532
7mers	13	1220
13mers	7	2252
27mers	3	4660

In Figure 7a, the intermolecular pair distribution function for the individual pairs of the same (Si−Si, CH_2-CH_2, CH_3-CH_3) types of interaction sites of PDMSTM is shown at 300 K. The $g_{CH_3-CH_3}(r)$ function has a pronounced peak at 4.4 Å, just above the contact distance value. The position of this peak is due to the fact that the methyl sites are more exposed to neighboring sites than either of the backbone sites, and the closest contact between two PDMSTM molecules is likely to refer to the methyl sites. The $g_{Si-Si}(r)$ function remains zero at distances greater than the distance of closest contact between two isolated Si sites. This behavior is a consequence of the shielding of the Si sites caused by the attached methyl groups. A similar behavior was observed at 350 and 400 K, with the exception that the intensity of the peaks decreased at higher temperatures.

In Figure 7b, the intermolecular pair distribution function for the individual pairs of the same interaction sites of PDMSM is shown. The distribution functions are similar to those of PDMSTM, although the peaks for PDMSM are lower for all $g(r)$ functions. This behavior is due to the presence of more substituents in PDMSM chains relative to PDMSTM chains. Therefore, segments belonging to different chains of PDMSM are unable to have as many intermolecular interactions as segments in PDMSTM chains, and so $g(r)$ functions exhibit lower peak values.

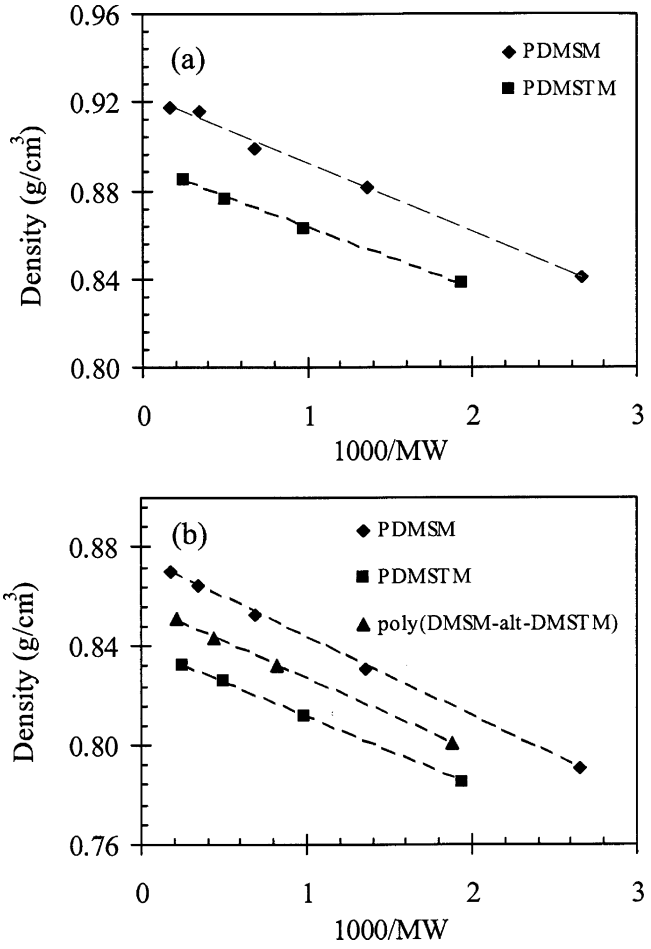

Figure 3. Molecular weight effect on the melt densities of PDMSM, PDMSTM, and poly(DMSM-*alt*-DMSTM) at 0.1 MPa at (a) 300 K and (b) 400 K as predicted from MD. The dashed lines correspond to the fit of eq 7.

The probability density for the two dihedral angles in the polymer backbone of PDMSTM, which are $CH_2-CH_2-CH_2-Si$ and $CH_2-CH_2-Si-CH_2$, is shown in parts a and b of Figure 8, respectively. For both angles, as temperature increases, peak heights decrease and distribution broadens, which is typical behavior for all chain fluids. The $CH_2-CH_2-CH_2-Si$ distribu-

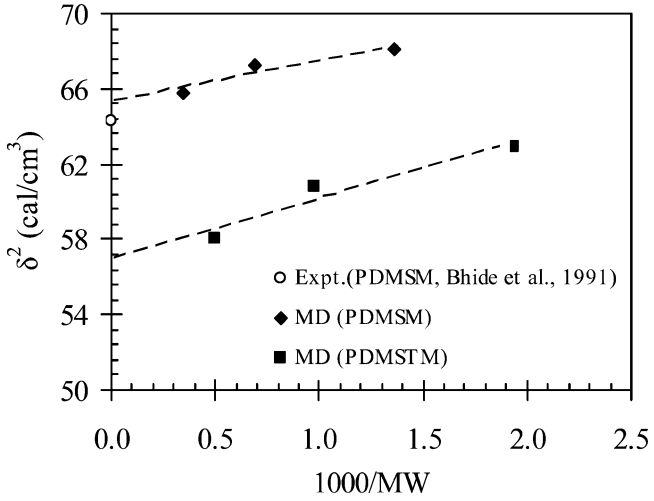

Figure 4. Molecular weight effect on the solubility parameter of PDMSM and PDMSTM at 300 K and 0.1 MPa.

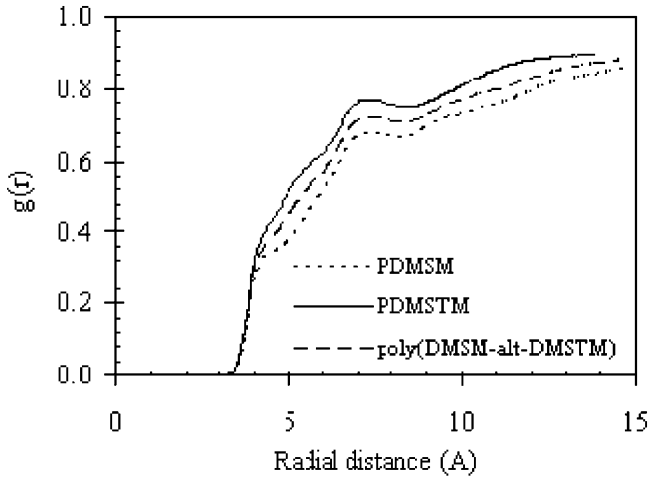

Figure 5. Total intermolecular pair distribution function for PDMSM, PDMSTM, and poly(DMSM-*alt*-DMSTM) from MD simulations at 300 K and 0.1 MPa.

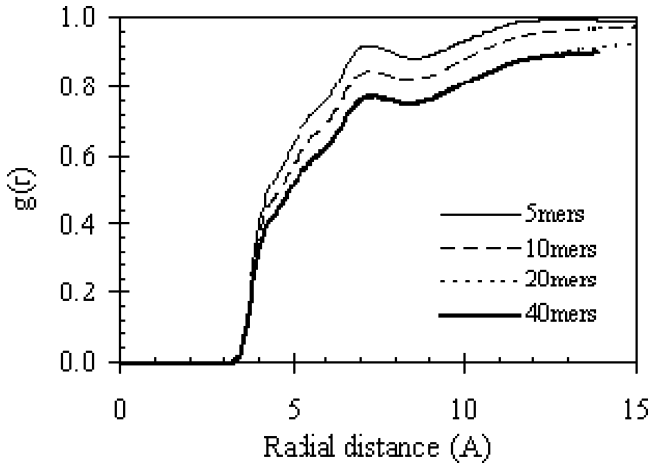

Figure 6. Total intermolecular pair distribution function for various molecular weights of PDMSTM at 300 K and 0.1 MPa from MD simulation.

tion shows a clear preference for the trans state (at 0°) with local maxima in the gauche$^+$ and gauche$^-$ conformations. This is a typical behavior for all *n*-alkanes, including polyethylene.[52] The exact positions of the gauche conformations are slightly shifted from the typical values of 120° and −120° by approximately 10°, respectively. This is due to the interaction of

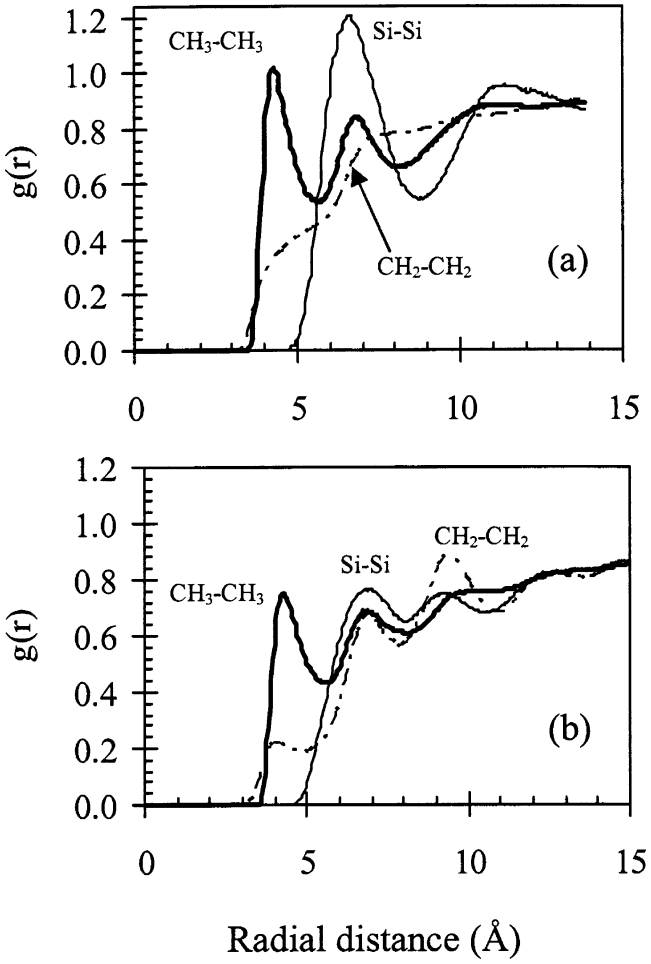

Figure 7. Intermolecular pair distribution function of the same types of interaction sites of (a) PDMSTM and (b) PDMSM at 300 K and 0.1 MPa from MD simulation.

the CH_3 UA attached to the Si atom with the first CH_2 UA of the $CH_2-CH_2-CH_2-Si$ subchain. This effect has already been observed during the ab initio calculations for TMSP,[29b] in the form of displaced local minima, and the present results confirm the force field's reliability.

The situation is different for the case of the second dihedral angle, $CH_2-CH_2-Si-CH_2$ (Figure 8b). In this case, all three conformations exhibit similar probability. This is due to the $2\pi/3$ periodicity characterizing the $CH_2-CH_2-Si(CH_3)_2-CH_2$ subchain torsion angles, given that identical local nonbonded parameter values are attributed to CH_2 and CH_3 UAs.

The dihedral angle probability density for PDMSM is similar to the probability density reported previously by Raptis et al.[24] and is not shown here. Furthermore, results for the copolymer are similar to the results for PDMSTM. There are no experimental data available for any of these polymers.

Results for the mean-square end-to-end distance $\langle R^2 \rangle$ as well as for the mean-square radius of gyration $\langle R_g^2 \rangle$ for all three polymers and for different chain lengths at 400 K and 0.1 MPa are presented in Table 6. For all chain lengths studied, except for the highest chain length for PDMSM, Flory's random coil hypothesis, that is, $\langle R^2 \rangle = 6\langle R_g^2 \rangle$, holds within the statistical uncertainty of the calculations. In the case of PDMSM, the mobility of the chains is much slower compared to the other two polymers. Much longer simulation runs would be needed to verify Flory's random coil hypothesis for this case, as well. Relatively larger fluctuations in $\langle R^2 \rangle$ and $\langle R_g^2 \rangle$ are observed for longer chains as a result of sample size effect (systems with

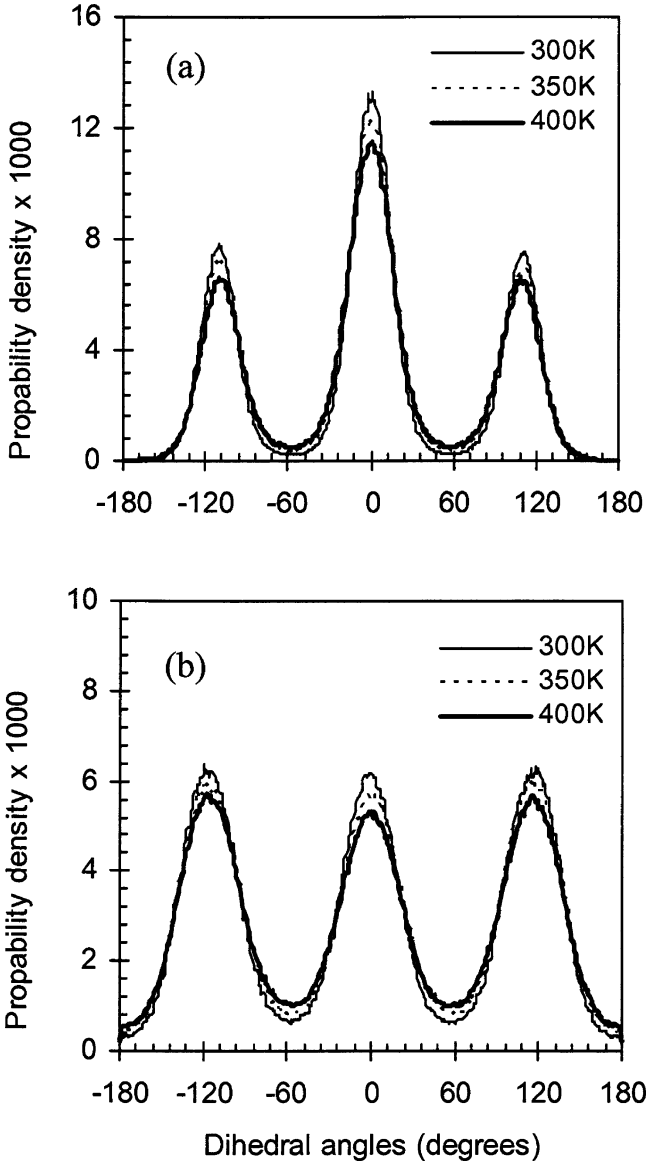

Figure 8. Distribution as a function of temperature of (a) $CH_2-CH_2-CH_2-Si$ and (b) $CH_2-CH_2-Si-CH_2$ dihedral angles of PDMSTM from MD simulation.

TABLE 6: Mean-Square End-to-end Distance, $\langle R^2 \rangle$, Mean-Square Radius of Gyration, $\langle R_g^2 \rangle$,and Their Ratio for Various Molecular Weight Values of PDMSM, PDMSTM, and poly(DMSM-*alt*-DMSTM) at 400 K and 0.1 MPa

chain size	$\langle R^2 \rangle$ (Å^2)	$\langle R_g^2 \rangle$ (Å^2)	$\langle R^2 \rangle / \langle R_g^2 \rangle$
	PDMSM		
5mers	112 ± 1	18.7 ± 0.1	6.0 ± 0.1
10mers	257 ± 22	42 ± 1	6.2 ± 0.3
20mers	587 ± 45	95 ± 3	6.2 ± 0.4
40mers	1055 ± 161	192 ± 15	5.5 ± 0.8
80mers	1362 ± 531	297 ± 43	4.5 ± 1.5
	PDMSTM		
5mers	204 ± 3	31.9 ± 0.3	6.4 ± 0.1
10mers	450 ± 48	71 ± 3	6.3 ± 0.4
20mers	867 ± 86	147 ± 9	5.9 ± 0.3
40mers	2107 ± 357	351 ± 32	6.0 ± 0.3
	poly(DMSM-*alt*-DMSTM)		
3mers	195 ± 7	31.1 ± 0.5	6.3 ± 0.1
7mers	568 ± 72	88 ± 6	6.4 ± 0.4
13mers	1021 ± 48	171 ± 99	6.0 ± 0.2

longer chain lengths consist of fewer chains) but also because chain relaxation requires a much longer time.

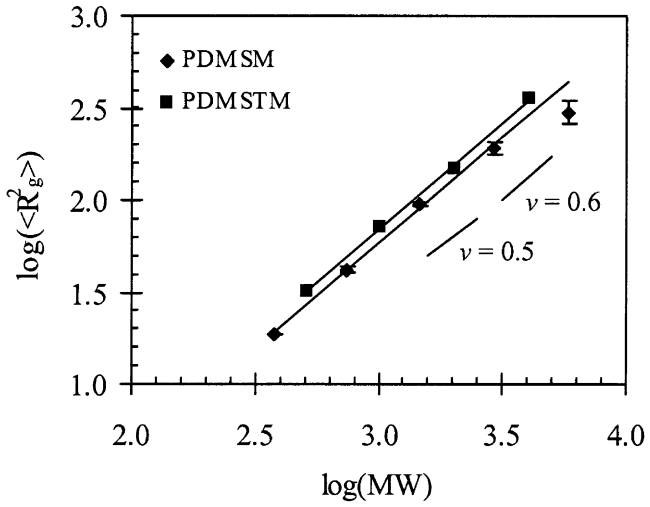

Figure 9. Double logarithmic plot of the mean-squared radius of gyration, $\langle R_g^2 \rangle$, of PDMSM and PDMSTM at 400 K and 0.1 MPa as a function of molecular weight. The solid lines depict the fit of eq 8. For comparison, short lines with $\nu = 0.5$ and with $\nu = 0.6$ are shown.

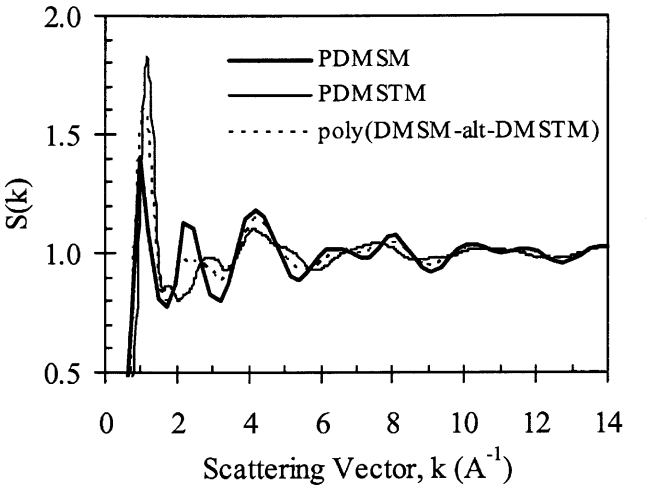

Figure 10. Static structure factor, $S(k)$, of PDMSM, PDMSTM, and poly(DMSM-*alt*-DMSTM) at 300 K and 0.1 MPa from MD simulation.

For polymer chains, the following scaling equation holds[52]

$$\langle R_g^2 \rangle^{1/2} \sim N^{\nu} \tag{8}$$

where N is the molecular weight of the polymer and ν is 0.5 for the case of unperturbed chains and 0.6 for the case of good solvent conditions. In general, polymer melts exhibit unperturbed chain behavior. In Figure 9, a double logarithmic plot of $\langle R_g^2 \rangle$ vs MW is shown for PDMSM and PDMSTM. Calculations for both polymers agree well with eq 8 with $\nu = 0.57 \pm 0.01$. For comparison, short lines with $\nu = 0.5$ and with $\nu = 0.6$ are shown in Figure 9. Polymer chains are more extended than expected, and this can be attributed to the relatively low molecular weight values examined. For larger chain sizes, ν is expected to approach 0.5.

Finally, the microscopic structure of the three polymers was examined by calculating the static structure factor that is based on the Fourier transform of the overall pair distribution function. The atomic scattering factors of Si, CH_2, and CH_3 were obtained from the literature.[53,54] In Figure 10, $S(k)$ for the polymers at 300 K and 0.1 MPa is shown as a function of the scattering vector, k. No experimental data are available for these polymers. The first peak in the static structure factor, at low k values,

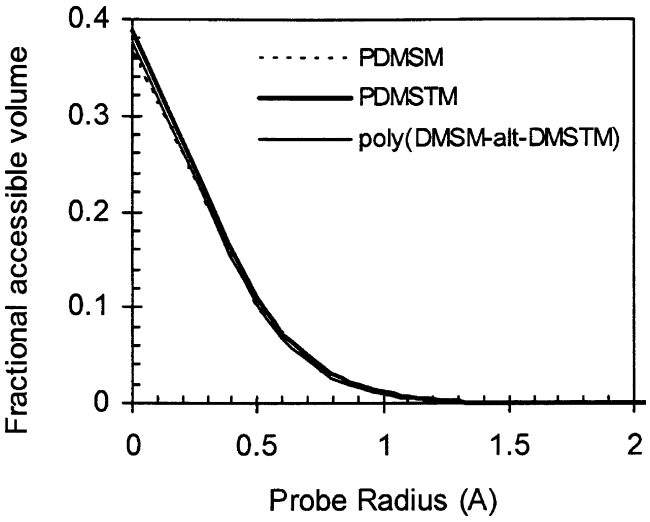

Figure 11. Fractional accessible volume of PDMSM, PDMSTM, and poly(DMSM-*alt*-DMSTM) as a function of penetrant radius at 300 K and 0.1 MPa from MD.

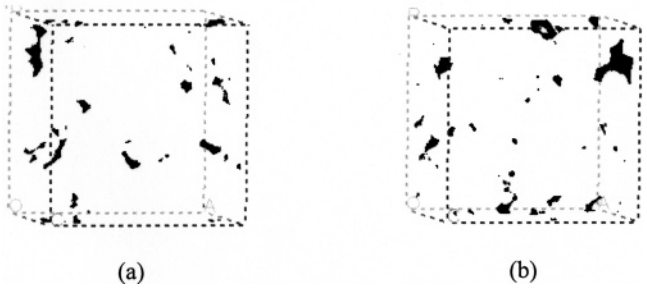

Figure 12. Clusters of volume accessible to an He molecule (r_p = 1.27 Å) for (a) PDMSM and (b) for PDMSTM at 300 K and 0.1 MPa.

corresponds to long-range intermolecular correlations, whereas the peaks at higher *k* values reflect intramolecular correlations. It is clear that the three polymers exhibit different intra- and intermolecular structures.

Free Volume Analysis. Characterization of polymer free volume is important to understand and further predict small molecule solubility and diffusion. In this work, the accessible volume of PDMSM, PDMSTM, and copolymer melts to small spherical penetrant molecules was calculated using the Greenfield and Theodorou approach.[55] Figure 11 depicts the fractional accessible volume as a function of penetrant radius for these polymers. The accessible volume decreases dramatically as the penetrant radius increases. The three polymers exhibit a similar accessible volume for a given penetrant molecular size. The accessible volume for a penetrant of zero radius corresponds to the average free volume fraction. The free volume fraction of PDMSTM is approximately 4% higher compared to the values of the other two polymers. This estimate is in agreement with the earlier conclusion that PDMSTM is less cohesive compared to PDMSM and to poly(DMSM-*alt*-DMSTM). Furthermore, in Figure 12, the volume accessible to a penetrant molecule of a size corresponding to an He atom (r_p = 1.27 Å) in one particularly equilibrated configuration of PDMSM and of PDMSTM obtained from *NPT* simulation is shown. Interestingly, the clusters of accessible volume are fewer for PDMSM.

C. Dynamic Properties. The local dynamics of the chains can be examined by monitoring the rate of reorientation of a unit vector, **u**, directed along the chain end-to-end vector with time. The following directional autocorrelation function is used to quantify the chain dynamics

$$P_2(t) = \frac{1}{2}\left(3\langle[\mathbf{u}(t)\cdot\mathbf{u}(0)]^2\rangle - 1\right) \tag{9}$$

As $P_2(t)$ approaches zero, the chain "forgets" its initial conformation and chain relaxation is achieved. Figure 13 refers to the decay of $P_2(t)$ for the different molecular weight samples of (a) PDMSTM and (b) PDMSM at 400 K, respectively. Obviously, relaxation time increases at higher molecular weights. MD simulations on the order of 150 ns real time were performed for the highest molecular weight value of PDMSM. PDMSM is shown to be "stiffer" (relaxes slower) than PDMSTM of the same molecular weight and at the same temperature. This is a consequence of the higher density, lower free volume, and higher cohesive energy density of PDMSM as quantified above. At lower temperatures (not shown here), relaxation time increases for all polymers.

The autocorrelation functions were fit to the Kohlrausch−Williams−Watts (KWW) equation[56]

$$P_{www}(t) = \exp\left(-\left(\frac{t}{\tau}\right)^{\beta}\right) \tag{10}$$

where τ is a characteristic decorrelation time and β is a stretching parameter. Decorrelation times for the various polymer melts as a function of molecular weight at 350 and 400 K are presented in Tables 7 and 8, respectively. A 50 K decrease in temperature results in an increase in decorrelation time for the end-to-end chain vector by a factor of 2−3.

The local dynamics of the chains can also be quantified in terms of the torsion autocorrelation function, defined as

$$P_{\varphi}(t) = \frac{\langle\cos\varphi(t)\cos\varphi(0)\rangle - \langle\cos\varphi(0)\rangle^2}{\langle\cos\varphi(0)^2\rangle - \langle\cos\varphi(0)\rangle^2} \tag{11}$$

The decay of $P_{\varphi}(t)$ for the three polymers at 300 K is shown in Figure 14. It is obvious that the PDMSTM melt and poly(DMSM-*alt*-DMSTM) exhibit almost the same rate of local conformational relaxation, while the mobility of PDMSM chains is appreciably slower compared to the other two polymers. In this case, a 50 K decrease results in an increase of the decorrelation time for local dynamics by a factor of 1.8−2.5.

The mean-square displacement of the chain center-of-mass $\langle R^2_{cm}(t)\rangle$ for the various PDMSTM samples at 400 K as a function of time, *t*, is displayed in Figure 15. A similar behavior was found at other temperatures and polymers as well. At time values sufficiently higher than the chain relaxation time, Fickian behavior is observed. In this way, the self-diffusion coefficient, *D*, can be calculated from the Einstein equation

$$D = \lim_{t\to\infty} \frac{\langle R^2_{cm}(t)\rangle}{6t} \tag{12}$$

The results are summarized in Tables 7 and 8. The uncertainties reported are the standard deviation of the three diagonal elements of the diffusion tensor (D_{xx}, D_{yy}, D_{zz}). In Figure 16, the self-diffusion coefficient as a function of molecular weight for (a) PDMSTM at 350 and 400 K and (b) PDMSM at 400 K is shown. The simulation data are fit accurately to the empirical equation[48]

$$D = kM^{-a} \tag{13}$$

where *k* and *a* are characteristic constants of the system. A least-squares fit results in the following values for exponent *a*: 1.7 ± 0.2 at 350 K and 1.8 ± 0.1 at 400 K for PDMSTM and 1.8

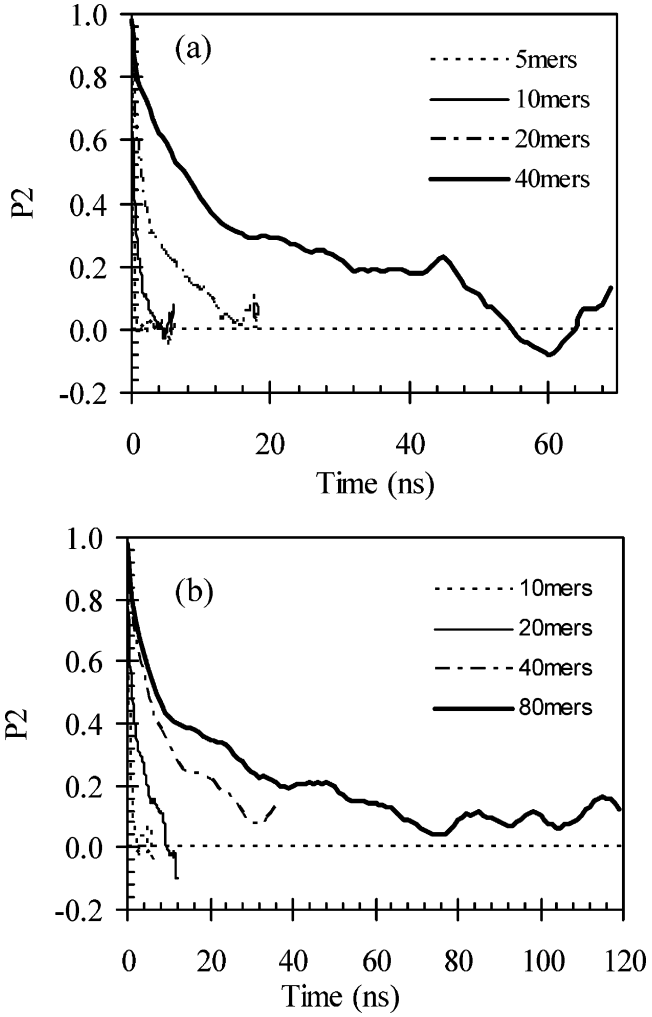

Figure 13. Time autocorrelation function, P_2, for the chain end-to-end vector for various chain lengths of (a) PDMSTM and (b) PDMSM at 400 K and 0.1 MPa from MD simulation.

TABLE 7: Decorrelation Time for the Chain End-to-end Vector and Self-diffusion Coefficient at 350 K for Various Molecular Weights of PDMSTM Melt

	τ (ps)	D (10^{-6} cm^2/s)
5mers	250	1.25 ± 0.32
10mers	2150	0.26 ± 0.07
20mers	10600	0.09 ± 0.04
40mers	35100	0.04 ± 0.02

$\pm$ 0.2 at 400 K for PDMSM. Theoretical models[57−59] as well as molecular simulations[60] have shown that, for short polymer chains, the Rouse model holds and $a = 1$, while for longer polymers, the reptation model prevails and $a = 2$. Consequently, the chain lengths examined here correspond to a transition regime, at least in terms of the dynamic properties.

5. Conclusions

In this work, a realistic UA force field was developed for the prediction of thermodynamic, structure, and dynamic properties of two silicon-containing polymers, which are poly(dimethylsilamethylene) and poly(dimethylsilatrimethylene) and their 50:50 alternating copolymer. Force-field development was based on recent ab initio quantum mechanics calculations on model monomers and dimers of these polymers for the calculation of bonded interactions and local intramolecular nonbonded interactions. For the intermolecular interactions and nonlocal nonbonded intramolecular interactions, existing force fields for similar compounds were used together with fitting to experimental thermodynamic data for one of the polymers at ambient conditions.

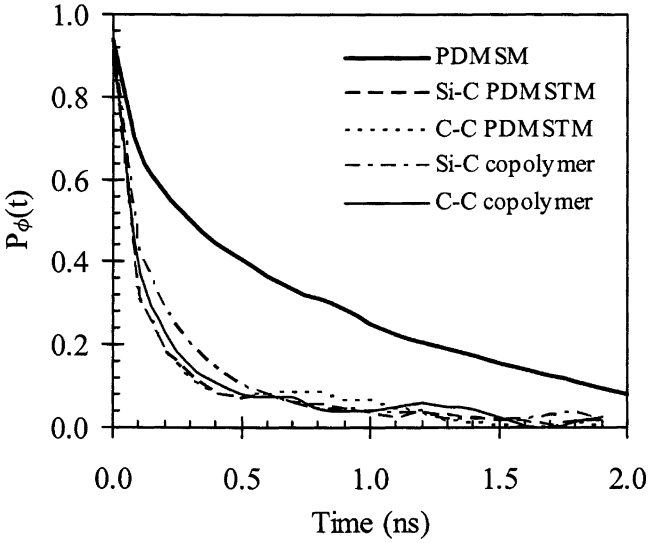

Figure 14. Torsional angle time autocorrelation function at 300 K and 0.1 MPa of PDMSM, PDMSTM, and poly(DMSM-*alt*-DMSTM) from MD simulation.

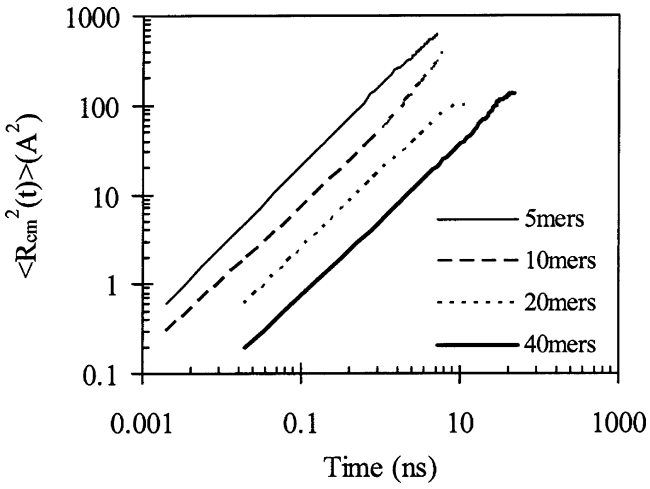

Figure 15. Chain center-of-mass mean-square displacement as a function of time for all chain lengths of PDMSTM at 400 K and 0.1 MPa.

TABLE 8: Decorrelation Time for the Chain End-to-end Vector and Self-diffusion Coefficient for Polymers of Various Molecular Weights at 400 K and 0.1 MPa

polymer	τ (ps)	D (10^{-6} cm^2/s)
PDMSM		
5mers	63	3.40 ± 0.25
10mers	460	0.80 ± 0.24
20mers	3250	0.38 ± 0.10
40mers	13150	0.13 ± 0.04
80mers	32200	0.02 ± 0.01
PDMSTM		
5mers	130	2.70 ± 0.34
10mers	770	0.91 ± 0.13
20mers	4100	0.20 ± 0.04
40mers	25000	0.07 ± 0.04
poly(DMSM-*alt*-DMSTM)		
3mers	144	2.32 ± 0.36
7mers	1250	0.62 ± 0.07
13mers	6800	0.24 ± 0.06

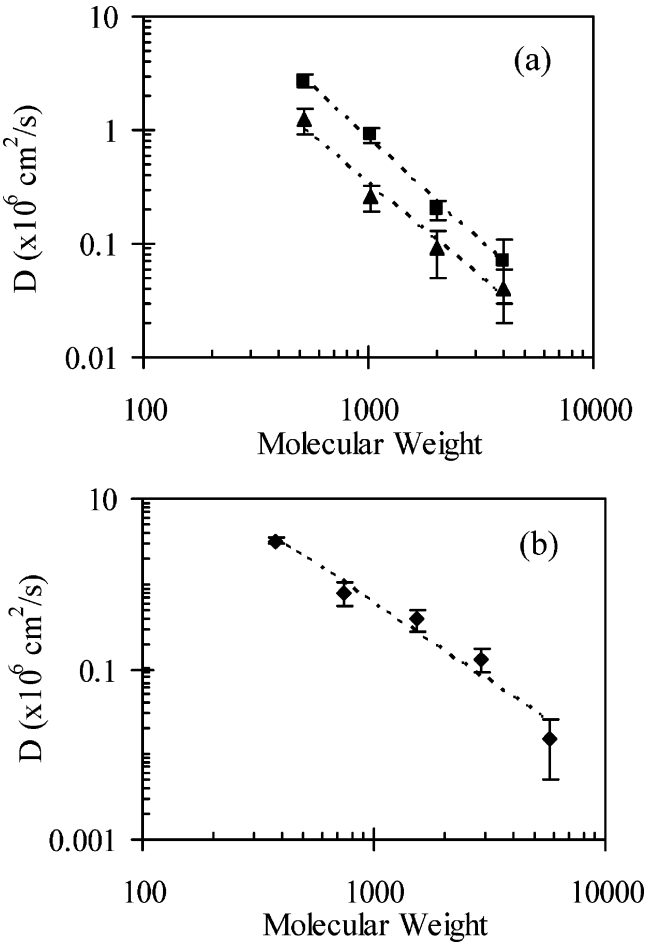

Figure 16. Chain center-of-mass self-diffusion coefficient, *D*, as a function of molecular weight MW for (a) PDMSTM melts at 350 K (triangles) and 400 K (squares) and (b) PDMSM at 400 K from MD simulations. The dotted lines depict the fit of eq 13.

Extensive *NPT* MD simulations were performed at different temperature and pressure conditions and for different polymer molecular weight values. Simulation results are in very good agreement with limited experimental thermodynamic data available at ambient conditions for PDMSM and the copolymer. Furthermore, simulation results are in very good agreement with widely used empirical macroscopic correlations for thermodynamic and structure properties of polymer melts. All polymer melts examined, with the exception of PDMSM's highest molecular weight, were shown to satisfy Flory's "random coil hypothesis". For the case of PDMSM 80mers, longer simulation runs would be needed.

Very long MD runs, some of them well above 100 ns, were performed to capture accurately the dynamic properties of the polymers. Characteristic relaxation times of the polymer chains were calculated, and the self-diffusion coefficient was evaluated. It was shown that, in the molecular weight range examined, polymer melts exhibit a transition behavior between the Rouse model and reptation model.

Currently, work is extended to mixtures of these polymers with low molecular weight hydrocarbons for the calculation of thermodynamic and transport properties. The ultimate goal of this work is the investigation of the separation properties of these polymers for multicomponent hydrocarbon mixtures.

Acknowledgment. Financial support of this project by the Greek General Secretariat of Research and Technology through the PENED 2003 program is gratefully acknowledged.

References and Notes

(1) Allen, M. P.; Tildesley, D. J. *Computer Simulation of Liquids*; Oxford Science Publications: Oxford, U.K., 1987.
(2) Frenkel, D.; Smit, B. *Understanding Molecular Simulation*, 2nd ed.; Academic Press: San Diego, CA, 2002.
(3) Colbourn, E. A., Ed. *Computer Simulation of Polymers*; Longman Group UK Ltd.: Essex, U.K., 1994.
(4) Kotelyanskii, M., Theodorou, D. N., Eds. *Simulation Methods for Polymers*; Marcel Dekker: New York, 2004.
(5) Landau, D. P.; Binder, K. *A Guide to Monte Carlo Simulations in Statistical Physics*; Cambridge University Press: Cambridge, U.K., 2000.
(6) Vacatello, M.; Avitabile, G.; Corradini, P.; Tuzi, A. *J. Chem. Phys.* **1980**, *73*, 548.
(7) Frenkel, D.; Mooij, G. C. A. M.; Smit, B. *J. Phys.: Condens. Matter* **1992**, *4*, 3053.
(8) Siepmann, J. I.; Frenkel, D. *Mol. Phys.* **1992**, *75*, 59.
(9) de Pablo, J. J.; Laso, M.; Suter, U. W. *J. Chem. Phys.* **1992**, *96*, 2395.
(10) Dodd, L. R.; Boone, T. D.; Theodorou, D. N. *Mol. Phys.* **1993**, *78*, 961.
(11) Pant, P. V. K.; Theodorou, D. N. *Macromolecules* **1995**, *28*, 7224.
(12) Karayiannis, N. Ch.; Mavrantzas, V. G.; Theodorou, D. N. *Phys. Rev. Lett.* **2002**, *88*, 105503.
(13) Peristeras, L. D.; Economou, I. G.; Theodorou, D. N. *Macromolecules* **2005**, *38*, 386.
(14) Karayiannis, N. Ch.; Mavrantzas, V. G. *Macromolecules* **2005**, *38*, 8583.
(15) Harmandaris, V. A.; Mavrantzas, V. G.; Theodorou, D. N. *Macromolecules* **1998**, *31*, 7934.
(16) Cuthbert, T. R.; Wagner, N. J.; Paulaitis, M. E.; Murgia, G.; D'Aguanno, B. *Macromolecules* **1999**, *32*, 5017.
(17) Hofmann, D.; Fritz, L.; Ulbrich, J.; Schepers, C.; Böhning, M. *Macromol. Theory Simul.* **2000**, *9*, 293.
(18) Putz, M.; Curro, J. G.; Grest, G. S. *J. Chem. Phys.* **2001**, *114*, 2847.
(19) Sides, S. W.; Curro, J.; Grest, G. S.; Stevens, M. J.; Soddemann, T.; Habenschuss, A.; Londono, J. D. *Macromolecules* **2002**, *35*, 6455.
(20) Makowska-Janusik, M.; Reis, H.; Papadopoulos, M. G.; Economou, I. G.; Zacharopoulos, N. *J. Phys. Chem. B* **2004**, *108*, 588.
(21) Stern, S. A.; Shah, V. M.; Hardy, B. J. *J. Pol. Sci. Pol. Phys.* **1987**, *25*, 1263.
(22) Shah, V. M.; Hardy, B. J.; Stern, S. A. *J. Pol. Sci. Pol. Phys.* **1993**, *31*, 313.
(23) Alentiev, A.; Economou, I. G.; Finkelshtein, E.; Petrou, J.; Raptis, V. E.; Sanopoulou, M.; Soloviev, S.; Ushakov, N.; Yampolskii, Y. *Polymer* **2004**, *45*, 6933.
(24) Raptis, V. E.; Economou, I. G.; Theodorou, D. N.; Petrou, J.; Petropoulos, J. H. *Macromolecules* **2004**, *37*, 1102.
(25) Economou, I. G.; Raptis, V. E.; Melissas, V. S.; Theodorou, D. N.; Petrou, J.; Petropoulos, J. H. *Fluid Phase Equilib.* **2005**, *228*−*229*, 15.
(26) Chen, D. H.; Mattice, W. L. *Polymer* **2004**, *45*, 3877.
(27) Martin, M. G.; Siepmann, J. I. *J. Phys. Chem. B* **1998**, *102*, 2569.
(28) Sok, R. M.; Berendsen, H. J. C.; van Gunsteren, W. F. *J. Chem. Phys.* **1992**, *96*, 4699.
(29) (a) Raptis, V. E.; Melissas, V. S. *J. Phys. Chem. B*, in press; (b) Raptis, V. E.; Melissas, V. S. Manuscript in preparation.
(30) Møller, C.; Plesset, M. S. *Phys. Rev.* **1934**, *46*, 618.
(31) McLean, A. D.; Chandler, G. S. *J. Chem. Phys.* **1980**, *72*, 5639. Krishnan, R.; Binkley, J. S.; Seeger, R.; Pople, J. A. *J. Chem. Phys.* **1980**, *72*, 650.
(32) Wollrab, J. E. *Rotational Spectra and Molecular Structure*; Academic Press: 1967. Kroto, H. W. *Molecular Rotation Spectra*; John Wiley: New York, 1975.
(33) Flory, P. J. *Statistical Mechanics of Chain Molecules*; John Wiley: New York, 1969.
(34) Sun, H. *Macromolecules* **1995**, *28*, 701.
(35) Holroyd, R. A.; Itoh, K.; Nishikawa, M. *Nucl. Instrum. Methods Phys. Res., Sect. A* **1997**, *390*, 233.
(36) Lide, D. R., ed. *Handbook of Chemistry and Physics*, 79th ed.; CRC Press: Boca Raton, FL, 1998−1999.
(37) Nosé, S.; Klein, M. L. *Mol Phys.* **1983**, *50*, 1055.
(38) Nosé, S. *J. Chem. Phys.* **1984**, *81*, 511.
(39) Nosé, S. *Mol. Phys.* **1984**, *52*, 255.
(40) Gear, C. W. *Numerical Initial Value Problems in Ordinary Differential Equations*; Prentice-Hall: Englewood Cliffs, NJ, 1971.
(41) Antoniadis, S. J.; Samara, C. T.; Theodorou, D. N. *Macromolecules* **1998**, *31*, 7944.
(42) Details can be found at www.accelrys.com/cerius2/.
(43) Theodorou, D. N.; Boone, T. D.; Dodd, L. R.; Mansfield, K. F. *Makromol. Chem., Theory Simul.* **1993**, *2*, 191.
(44) Chakraborty, A. K.; Theodorou, D. N. *Applied Molecular Theory for Chemical Engineers*; Oxford University Press, in preparation.

(45) Soloviev, S. A.; Yampolskii, Yu. P.; Economou, I. G.; Ushakov, N. V.; Finkelshtein, E. Sh. *Polym. Sci. Ser. A.* **2002**, *44*, 293.
(46) Ko, J. H.; Mark, J. E. *Macromolecules* **1975**, *8* (6), 869; **1975**, *8* (6), 874.
(47) Bhide, B. D.; Stern, S. A. *J. Appl. Polym. Sci.* **1991**, *42*, 2397.
(48) van Krevelen, D. W. *Properties of Polymers*, 3rd ed.; Elsevier: Amsterdam, The Netherlands, 1990.
(49) Theodorou, D. N.; Suter, U. W. *Macromolecules* **1985**, *18*, 1467.
(50) Mavrantzas, V. G.; Boone, T. D.; Zervopoulou, E.; Theodorou, D. N. *Macromolecules* **1999**, *32*, 5072.
(51) Doxastakis, M.; Mavrantzas, V. G.; Theodorou, D. N. *J. Chem. Phys.* **2001**, *115*, 11339.
(52) Mattice, W. L.; Suter, U. W. *Conformational Theory of Large Molecules*; Wiley: New York, 1994.
(53) Narten, A. H. *J. Chem. Phys*. **1979**, *70*, 299.
(54) Iber, J. A., Hamilton, W. C., Eds. *International Tables for X-ray Crystallography*; Kluwer Academic Publishers: Boston, MA, 1989; Vol. IV (Revised and Supplementary Tables), Table 2.2A.
(55) Greenfield, M. L.; Theodorou, D. N. *Macromolecules* **1993**, *26*, 5461.
(56) Matsuoka, S. *Relaxation Phenomena in Polymers*; Hanser Publishers: Munich, Germany, 1992.
(57) De Gennes, P. G. *J. Chem. Phys.* **1971**, *55*, 572.
(58) De Gennes, P. G. *J. Chem. Phys.* **1980**, *72*, 4756.
(59) Doi, M.; Edwards, S. F. *The Theory of Polymer Dynamics*; Clarendon: Oxford, U.K., 1986.
(60) Kremer, K.; Grest, G. S.; Carmesin, I. *Phys. Rev. Lett.* **1988**, *61*, 566.